Earthquakes and Structures, Vol. 3, No. 3-4 (2012) 297-313
DOI: http://dx.doi.org/10.12989/eas.2012.3.3.297

A time domain analysis of train induced vibrations

A. Romero, P. Galvín* and J. Domínguez

Escuela Técnica Superior de Ingeniería, Universidad de Sevilla, Camino de los Descubrimientos, 41092 Sevilla, Spain

(Received December 7, 2011, Revised February 27, 2012, Accepted April 10, 2012)

Abstract. This paper is intended to show the robustness and capabilities of a coupled boundary element-finite element technique for the analysis of vibrations generated by high-speed trains under different geometrical, mechanical and operation conditions. The approach has been developed by the authors and some results have already been presented. Nevertheless, a more comprehensive study is presented in this paper to show the relevance and robustness of the method which is able to predict vibrations due to train passage at the vehicle, the track, the free-field and any structure close to the track. Local soil discontinuities, underground constructions such as underpasses, and coupling with nearby structures that break the uniformity of the geometry along the track line can be represented by the model. Non-linear behaviour of the structures can be also considered. Results concerning the excitation mechanisms, track behaviour and sub-Rayleigh and super-Rayleigh train speed are summarized in this work.

Keywords: FE/BE model; time domain; HST vibration

1. Introduction

The emergence of high-speed trains (HST) has proven to be one of the most significant technological advances in transportation industry of the last part of the twentieth century and the beginning of the twenty-first (Banister and Hall 1993). Engineers interest for soil vibrations due to high-speed moving loads has grown in the last two decades. This interest has been induced by the increasing importance of HST in modern transportation. Many new HST lines are being constructed in Europe, Asia and the USA. Moreover, new slab track installations are being developed in Europe and Asia for low maintenance cost in high-speed passenger and heavy-load freight service lines. This innovative concrete slab could replace the classical ballast track (Esveld 2001).

HSTs have greatly improved inter-city transportation, but at the same time have given rise to certain problematic issues which should be addressed. The passage of HST induces vibrations which are transmitted through the track into the soil, reaching levels that can cause significant soil displacement and excessive distortion in the track. Also, the vibration generated by the operation of rail system is a source of disturbance for people who live or work in buildings near the lines. These effects require a deep analysis in order to maintain security and comfort in the trains, and to avoid problems in nearby constructions due to vibrations induced by waves propagated through the soil. The study of soil-induced motion requires comprehensive models that take into account many

*Corresponding author, Ph.D., E-mail: pedrogalvin@us.es

factors related to the source (train), the transmission medium (soil) and the receptor (buildings).

One of the first steps in the study of vibrations induced by HST is an accurate modelling of the force induced by the train which is transmitted to the soil through the track. This force is generated by several excitation mechanisms: the quasi-static contribution (force generated by moving axle loads), the parametric excitation due to discrete supports of the rails, the transient excitation due to rail joints and wheel flats, and the excitation due to track unevenness (Hauck *et al*. 1996). In the early studies, a prediction model developed by Krylov (1995) was used by the authors (Galvín and Domínguez 2007a, 2007b). In that model, only the quasi-static force transmitted by the sleepers in a ballasted track was taken into account as a moving force. Recently, more advanced models have been used by the authors allowing the dynamic train-track interaction mechanisms and the actual track properties to be considered (Galvín and Domínguez 2009, Galvín *et al*. 2010a, 2010b).

The finite element method (FEM) and the boundary element method (BEM) are well suited numerical techniques for the study of induced vibrations due to HST. It is known that boundary element method is well suited for dynamic soil-structure interaction problems since unbounded regions are represented in a natural way (Domínguez 1993) and local conditions can be represented without many difficulties. FEM is best suited for solving problems with inhomogeneities and non-linearity (Zienkiewicz 1986). In the last years, several models have been developed. Lombaert *et al*. (Lombaert *et al*. 2006, Lombaert and Degrande 2009) have applied the formulation presented by Metrikine *et al*. (2005), Metrikine and Popp (1999) and Dieterman and Metrikine (1996), to predict vibrations produced by railway traffic using a coupled two-and-half dimensional boundary element-finite element formulation in the frequency domain. In that approach the vehicle is coupled to an infinite length beam that represents the track and a half-space representing the soil. The model has been validated by experimental results (Lombaert *et al*. 2006, Lombaert and Degrande 2009). Auersch (2008, 2005) has presented a model for ground-borne railway induced vibrations formulated in a similar way. Takemiya and Bian (2005) have extended the model presented by Metrikine and Popp (1999) to consider the facts that rails are based discretely on the ground and sleepers have a significant inertia effect on the rails. They included a layered soil in the analysis and used a discrete Kelvin model for the sleepers' complex frequency-dependent stiffness. Sheng *et al*. (2003, 2004, 2006) also applied a two-and-a-half dimensional frequency domain model to study vibrations due to train passage. In that model, the dynamic train-track interaction is taken into account using an infinite layered beam for the track coupled to a layered half-space. Galvín *et al*. (2010) have presented a comprehensive 2.5*D* model where the track-soil interaction is taken into account in a rigorous way. Xia *et al*. (2010) have presented an integrated train-track-subsoil dynamic interaction model for train induced ground vibration based on vehicle dynamics, track dynamics and Green's functions of the soil. The previous numerical models, except reference (Xia *et al*. 2010), are formulated in the two-and-a-half dimensional domain; therefore, it is supposed that the ground and structures such as tunnels and tracks are homogeneous in the track direction. These models use Green's functions for a layered full space or for a layered half-space to represent the soil.

The authors have developed a general and fully coupled three-dimensional multi-body-finite element boundary element model formulated in the time domain to predict vibrations due to train passage at the vehicle, the track, the free field and structures situated near the track. The model has been developed to account for the full dynamic vehicle-track-soil interaction. As compared to two-and-a-half dimensional domain solutions, the formulation developed could be used to take into account local soil discontinuities, underground constructions such as underpasses, and coupling with nearby structures that break the uniformity of the geometry along the track line. Previous studies (Olmos and

Roësset 2010) show clearly the importance of the non-linear behavior on the dynamic performance of structures. Non-linear behaviour could be also considered in the proposed model since a time domain formulation is employed (Zienkiewicz 1986). However, the main disadvantage of the three-dimensional models is that they are computationally expensive.

In this paper, main and most relevant results obtained along the last years are presented and summarized (Galvín and Domínguez 2007a, 2007b, 2009, Galvín *et al*. 2010a, 2010b). First, the numerical model is briefly presented. The model is based on three-dimensional finite element (Zienkiewicz 1986) and boundary element (Domínguez 1993) time domain formulations. A direct procedure is used to couple boundary and finite element methods (Karabalis and Beskos 1985, Estorff and Pabrucki 1990). A multi-body model is considered to represent the vehicle. The quasi-static and the dynamic load components are analysed. Second, ballasted and non-ballasted tracks are studied: the effects of ballast and embankment geometry are evaluated, track recepentances are computed for different track systems and vibrations induced by high-speed train passages at the track and the free field are evaluated for different train speeds. Then, the dynamic behaviour of a transition zone between a ballast track and a slab track is analysed. Finally, the dynamic response of a short span bridge is studied.

2. Numerical model

The boundary element system of equations can be solved step-by-step to obtain the time variation of the boundary unknowns, i.e., displacements and tractions. Piecewise constant time interpolation functions are used for tractions and piecewise linear functions for displacements. The fundamental displacement and traction solutions are evaluated analytically without much difficulty, and nine nodes rectangular and six node triangular quadratic elements are used for spatial discretization. Explicit expressions of the fundamental displacement and traction solutions corresponding to an impulse point load in a three-dimensional elastic full space can be seen in reference (Galvín and Domínguez 2007b). An approach based on the idea of using a linear combination of equations for several time steps in order to advance one step is used to ensure that the stepping procedure is stable in time. Details of this stabilization approach can be found in (Marrero and Domínguez 2003).

Once the integral equation is discretized one obtains the following equation for each time step

$$H^{nn}u^{n} = G^{nn}p^{n} + \sum_{m=1}^{n-1}(G^{nm}p^{m} - H^{nm}u^{m})\,exp[-2\pi\alpha(n-m)\Delta t] \tag{1}$$

where $\mathbf{u}^n$ is the displacement vector and $\mathbf{p}^n$ is the traction vector at the end of the time interval n, and $\mathbf{H}^{nn}$ and $\mathbf{G}^{nn}$ are the full unsymmetrical boundary element system matrices, in the time interval n, α is the soil attenuation coefficient and Δt is the time step. The right hand side term derived from previous steps is damped by an exponential coefficient using a linearly increasing exponent with time (Galvín and Domínguez 2007a).

Usually, the Spectral Analysis of Surface Waves (SASW) is used to determinate the dynamic soil properties at the studied site. In this test, ground vibrations are generated by means of hammer impacts on a foundation. The response is measured at several points at the soil's surface. The soil's damping coefficient α can be estimated from these measurements solving an inverse problem (a minimization procedure where the variable is α).

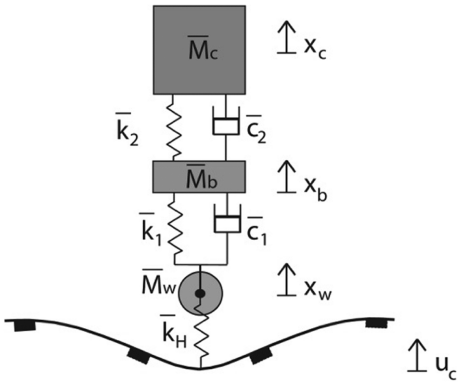

Fig. 1 The multi-body model for an axle

The equation which results from the finite element method can be expressed symbolically as follows if an implicit time integration Newmark method is applied (Newmark 1959).

$$D^{nn}u^{n} = f^{n}+f^{n-1} \tag{2}$$

where $\mathbf{D}^{nn}$ is the dynamic stiffness matrix, $\mathbf{u}^{n}$ the displacement vector and f^{n} the equivalent force vector, in the time interval n.

The multi-body model shown in Fig. 1 is used to represent the train-track dynamic interaction due to an axle passage (Galvín *et al*. 2010a). The primary and secondary suspensions isolate the carriages from the track vibrations. The axles and the car body are considered as rigid parts and the primary and secondary suspensions are represented by spring and damper elements (Sheng *et al*. 2004).

Coupling boundary element and finite element sub-regions entails satisfying equilibrium and compatibility conditions at the interface between both regions.

3. Quasi-static and dynamic excitation mechanisms

In the early studies, a prediction model developed by Krylov (1995, 1994) was used (Galvín and Domínguez 2007a, 2007b). In that model, only the quasi-static force transmitted by the sleepers to ballasted track was taken into account as a moving force. Krylov's model is valid when the train speed is close to the critical phase velocity of the coupled track-soil system because in this case the quasi-static excitation is dominant (Lombaert *et al*. 2006, Auersch 2008, Sheng *et al*. 2003).

After, more advanced models have been used allowing the dynamic train-track interaction mechanisms and the actual track properties to be considered (Fig. 1).

The random track unevenness $u_{w/r}(y)$ is modelled as a stationary Gaussian random process characterized by its one-sided PSD function $\tilde{S}_{u_{w/r}}(k_y)$. The spectral representation theorem is used to generate samples of track unevenness $u_{w/r}(y)$ as a superposition of harmonic functions with random phase angles (Lombaert *et al*. 2006, Lombaert and Degrande 2009).

$$u_{w/r}(y) = \sum_{m=1}^{n} \sqrt{2\tilde{S}_{u_{w/r}}(k_{ym})\Delta k_y}\cos(k_{ym}y-\theta_m) \tag{3}$$

where $k_{ym} = m\Delta k_y$ is the wavenumber sampling used only to compute the artificial profile, Δk_y the wavenumber step, and θ_m the independent random phase angles uniformly distributed in the interval $[0, 2\pi]$.The artificial track profile is generated from PSD function according to ISO 8608 (1995)

$$\tilde{S}_{u_{w/r}}(k_y) = \tilde{S}_{u_{w/r}}(k_{yo})\left(\frac{k_y}{k_{yo}}\right)^{-w} \tag{4}$$

The quasi-static and dynamic excitation mechanisms due to the vehicle response, the sleeper discrete support and the rail and wheel unevenness are all analysed (Galvín *et al*. 2010a). Fig. 2(a) shows the cross section of a classical ballast track that it is represented by the mesh shown in Fig. 2(b). The track is composed of two UIC60 rails with a bending stiffness $El = 6.45 \times 10^6$ Nm^2 and a mass per unit length $m = 60.3$ kg/m for each rail. The rail pads have a thickness of 10 mm and their stiffness and damping values are $k_{rp} = 150 \times 10^6$ N/m and $c_{rp} = 13.5 \times 10^3$ Ns/m, respectively. The pre-stressed concrete mono-block sleepers have a length $l = 2.60$ m, a width $w = 0.235$ m, a height $h = 0.205$ m and a mass $m = 300$ kg. A distance $d = 0.6$ m between the sleepers is considered. The ballast has a density $\rho = 1500$ kg/m^3, a Poisson ratio $v = 0.2$ and a Young's modulus equal to $E = 200 \times 10^6$ N/m^2. The width of the ballast and subballast layer equals 2.92 m and the height $h = 1.00$ m. The track is assumed to be located at the surface of a homogeneous half-space that represents the soil, with a *S*-wave velocity $C_s = 150.0$ m/s, a *P*-wave velocity $C_p = 300$ m/s and a Rayleigh wave velocity $C_R = 139.7$ m/s.

The quasi-static response due to the passage of a single axle can be obtained considering the unevenness term $u_{w/r}$ equal to zero. Since the sleepers are included in the model, the dynamic effects due to discrete rail support are considered implicitly. Fig. 3 shows the time history of the vertical displacement and the vertical velocity and the frequency content of the vertical velocity at

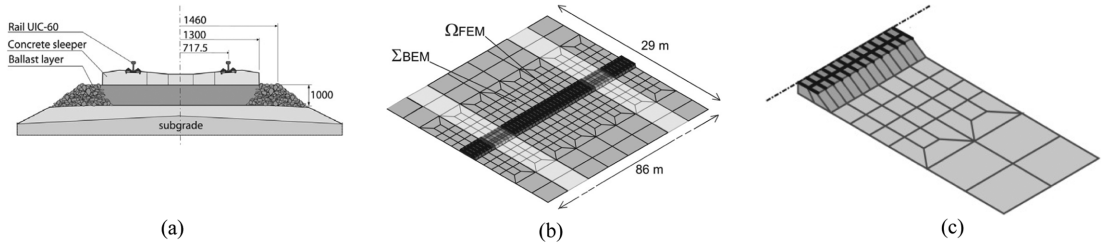

Fig. 2 (a) Ballast system track, (b) track and soil discretization and (c) detail of the discretization

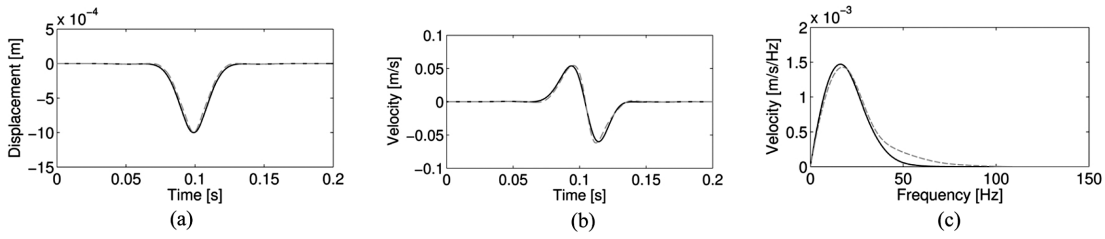

Fig. 3 (a) Time history of the vertical displacement, (b) vertical velocity and (c) frequency content of the vertical velocity of the rail for a single axle travelling at $v = 298$ km/h computed with the moving force model (black line) and the multi-body model (dashed grey line)

the rail for a single axle travelling at $v = 298$ km/h computed with a model where only a moving force is considered and with the multi-body model.

The displacement shown in Fig. 3(a) is completely symmetric. The vertical displacement and velocity at the rail computed from both models have similar values. The main differences are due the inertia is neglected in the moving force model, as can be seen in the computed frequency content of the vertical velocity (Fig. 3(c)). Both models lead to the same solution only when the axle speed is low or if the primary vertical stiffness tends to zero (Pesterev *et al*. 2003). Therefore, the vehicle model should be considered to predict the quasi-static response.

Fig. 4 shows the time history and the frequency content of the vertical displacement of the car body due to the moving axle and the parametric excitation due to the discrete supports of the rails for a single axle travelling at $v = 36$ km/h and at $v = 298$ km/h. The sleeper position is shown by vertical lines. It is clearly observed that the maximum displacements of the car body occur when the axle is approximately in the middle between two sleepers and the minimum when the axle is on the sleeper in accordance to the lower and higher stiffness of the track in those zones, respectively.

In order to investigate the behaviour of the coupled vehicle-track-soil system due to rail and wheel unevenness, the dynamic response due to the passage of a single axle train can be obtained if gravity is neglected. Again, the sleepers are included in the model and, therefore, the dynamic effects due to discrete rail support are also taken into account. An artificial track profile is generated from the PSD function according to ISO 8608 by Eq. (4) with $k_{y0} = 1$ rad/m, $w = 3.5$ as commonly

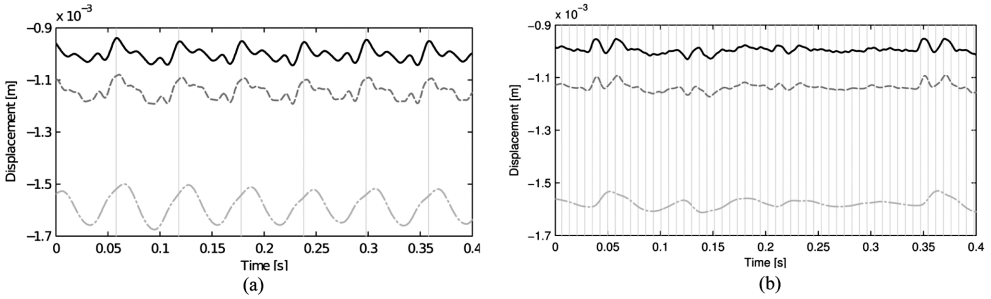

Fig. 4 Time histories of the vertical displacement of the car body (dashed-dotted light grey line), boogie (dashed dark grey line) and wheel (solid black line) due to discrete sleeper support for a single axle travelling at (a) $v = 36$ km/h and (b) $v = 298$ km/h. The sleepers positions are shown as vertical grey lines

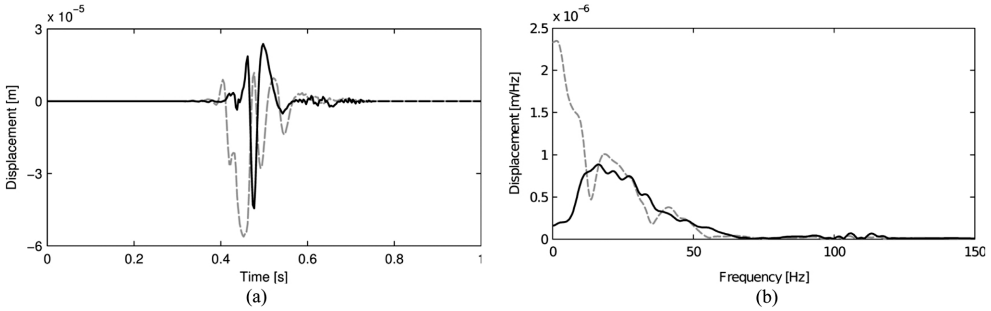

Fig. 5 (a) Time history and (b) frequency content of the vertical displacement of the rail for a single axle travelling at $v = 298$ km/h computed with the unsprung mass model (black line) and the multi-body model (dashed grey line)

assumed for railway unevenness, and a value of $\tilde{S}_{u_{w/r}}(k_{y0}) = 2\pi \times 10^{-8}$ m^3.

It is commonly adopted in the literature (Lombaert *et al*. 2006, Lombaert and Degrande 2009, Knothe and Grassie 1993) that the influence of the suspended mass can be neglected and the vehicle's unsprung mass is the only component that affects the dynamic loads due to the rail and wheel unevenness. The consistency of the previous hypothesis is studied from the results presented in Fig. 5 where the time history and the frequency content of the vertical displacement of the rail due to unevenness for a single axle travelling at $v = 298$ km/h computed with the unsprung mass model and the multi-body model, respectively, are shown. Both models lead to a similar response for frequencies higher than 10 Hz approximately. Therefore, the model could be simplified as at frequencies of more than a few Hertz (Knothe and Grassie 1993) since the vehicle's primary and secondary suspension isolate the body and the boogie from the wheel-set. A maximum rail displacement occurs between 10 and 40 Hz for both models that corresponds to the resonance frequency of the vehicle model or the unsprung mass model on the track. However, at lower frequencies, the suspended mass should be taken into account in order to predict the track and soil response accurately.

4. Ballasted and non-ballasted tracks

4.1 Ballast and embankment effects

Ballast and train-track embankment geometry and properties play an important role on the soil motion due to high-speed train passage (Galvín and Domínguez 2007a). Their effects can be evaluated by representing the actual ballast and embankment geometry and properties using the model summarized in this paper. In order to asses this effect, a simple geometry and loading situation is studied to validate the proposed approach. Consider a homogeneous soil and a 0.8 m thick embankment with geometry as shown in Fig. 6. This problem was studied by Adam *et al*. (2000) using 2-D and 3-D approaches. Following Adam *et al*. (2000) and in order to use their results for comparison, the train track load is represented by two impulse line loads with amplitude 10^3 N/m that last for 0.02 s which are applied where the two beam rails are located. Mass density $\rho = 2000$ kg/m^3 and a Poisson's ratio $v = 1/3$ are assumed to be identical for embankment and half-space.

Two cases are evaluated for comparison purposes. In Case 1 the *S*-wave velocity is the same for embankment and half-space ($C_s = 250$ m/s); in Case 2, $C_s = 250$ m/s for the embankment and

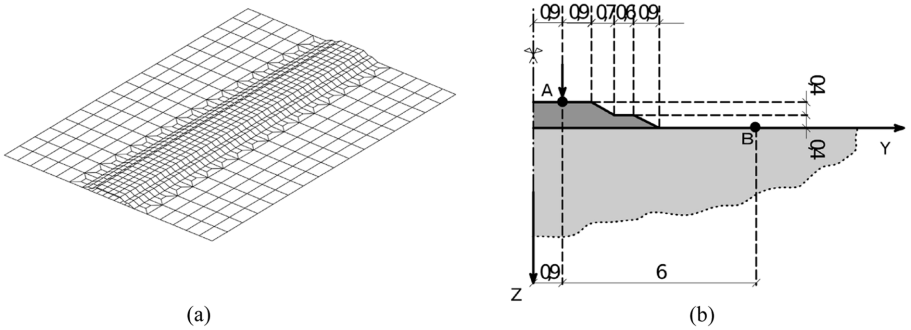

(a) (b)

Fig. 6 Half-space with 0.8 m thick ballast embankment. *BE* discretization and geometry

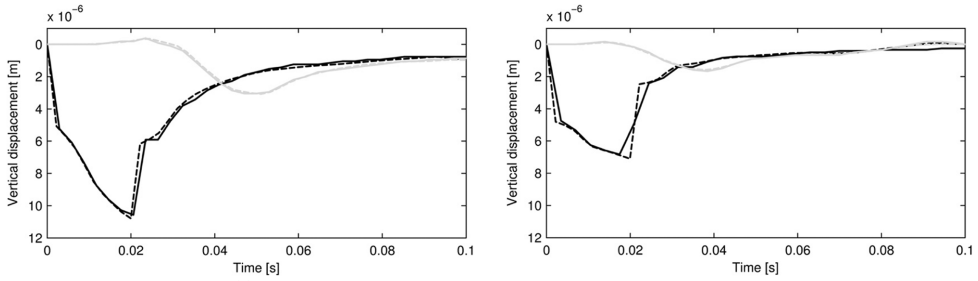

Fig. 7 Vertical displacement at points *A* (solid black line) and *B* (solid grey line). Results presented by Adam *et al*. (2000) are represented by dashed lines: (a) Case 1 and (b) Case 2

$C_s = 400$ m/s for the half-space. Soil surface vertical displacements at two points *A* and *B* are represented in Figs. 7(a) and 7(b). *A* is located under the load (the rail line) and *B* on the half-space surface 6 m from the rail. Figs. 7(a) and 7(b) show computed vertical displacement time history for Case 1 and Case 2, respectively. Results are in very good agreement with those obtained by Adam *et al*. (2000). Figs. 7(a) and 7(b) show a vertical displacement under the load line (point *A*) that increases with time as the load is applied ($0\text{ s} \leq t < 0.02\text{ s}$). Once the load is withdrawn, the vertical displacement under the load line goes to zero as it does for a quasi-static load ($t > 0.02$ s). Straight line segments in Figs. 7(a) and 7(b) are due to the time integration process. As pointed out in (Adam *et al*. (2000)), apart from the little kinks due to wave scattering at the embankment edges, the soil response for Case 1 is very similar to that of a half-space since the only difference is in the surface profile. A positive maximum of the vertical displacement corresponding to the first *S*-wave arrival time is observed in Fig. 7(a) for the point at 6 m from the load (point *B*). After that time, vertical displacement at point *B* decreases to the minimum value when the effect of the load withdrawal is noticed at that point (Rayleigh waves from the nearest loading point). The vertical displacement peak values at both points are smaller in Case 2 than in Case 1 as could be expected for a stiffer half-space.

4.2 The track dynamic response

The track receptance is computed as a function of the frequency for three different track systems: ballasted track, slab track and floating slab track (Galvín *et al*. 2010b). To this end, the systems are subjected to a series of unit amplitude sinusoidal excitations applied at both rails. The response time history is computed using the discretizations show in Fig. 8. The frequency content of the response is used to define the receptance.

The rail, rail pads and sleeper properties are as presented in Section 3. Fig. 8(a) shows a classical ballast track. The resilience of the track is due to two layers: a ballast layer on a sub-ballast layer. The ballast has a Young's modulus $E_b = 280 \times 10^6$ N/m^2, a shear modulus $G_b = 116 \times 10^6$ N/m^2 and a density $\rho_b = 1500$ kg/m^3. The sub-ballast layer has a Young's modulus $E_{sb} = 140 \times 10^6$ N/m^2, a shear modulus $G_{sb} = 58 \times 10^6$ N/m^2 and a density $\rho_{sb} = 1500$ kg/m^3. The damping value in both layers is $c_b = 24 \times 10^3$ Ns/m^2. The width of the ballast equals 2.92 m and the height $h_b = 0.7$ m.

The slab track system is composed of a concrete slab on a hydraulic sub-base (Fig. 8(b)). The concrete slab has a Young's modulus $E_s = 34 \times 10^9$ N/m^2, a shear modulus $G_s = 14.2 \times 10^9$ N/m^2 and a density $\rho_s = 2500$ kg/m^3. The hydraulic sub-base has a Young's modulus $E_{hs} = 10\times 10^9$ N/m^2, a shear

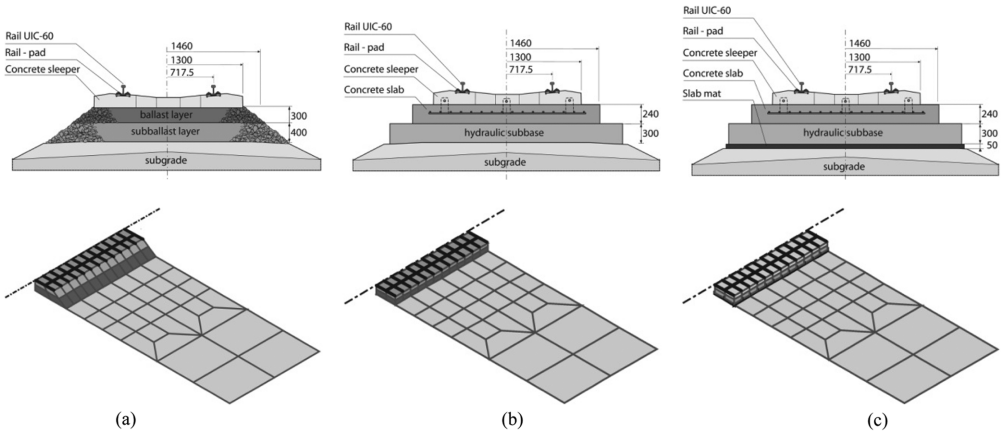

Fig. 8 Cross section and discretization detail for: (a) ballasted track, (b) slab track and (c) floating slab track

modulus $G_{hs} = 4.2 \times 10^9$ N/m^2, a density $\rho_{hs} = 2500$ kg/m^3 and the same width as the concrete slab.

In the case of the floating slab track, a mat is considered under the slab (Fig. 8(c)). The mat has a Young's modulus $E_f = 0.5 \times 10^6$ N/m^2, a density $\rho_f = 100$ kg/m^3 and a damping value $c_f = 87.6 \times 10^3$ Ns/m^2. For a floating slab track, the isolation frequency is defined as the resonance frequency of a single-degree-of-freedom system with a mass equal to the slab's mass per unit length and stiffness equal to the vertical stiffness of the slab bearings

$$f = \frac{1}{2\pi}\sqrt{\frac{k_f}{m_s}} \tag{5}$$

In this case, if m_s is the mass of the concrete slab and the hydraulic sub-base, the isolation frequency equals 13.69 Hz.

The tracks are located at the surface of a homogeneous half-space that represents a soft soil, with a *S*-wave velocity $C_s = 80$ m/s, a *P*-wave velocity $C_p = 150$ m/s and a Rayleigh wave velocity $C_R = 74$ m/s. The *S*-wave velocity in the soil is closed to the train speed; therefore, the critical speed for trains on ballast track could be reached.

Fig. 9 shows the track receptance for the ballast track, the (unisolated) slab track and the (isolated) floating slab track. The different flexibility of the tracks plays an important role on the

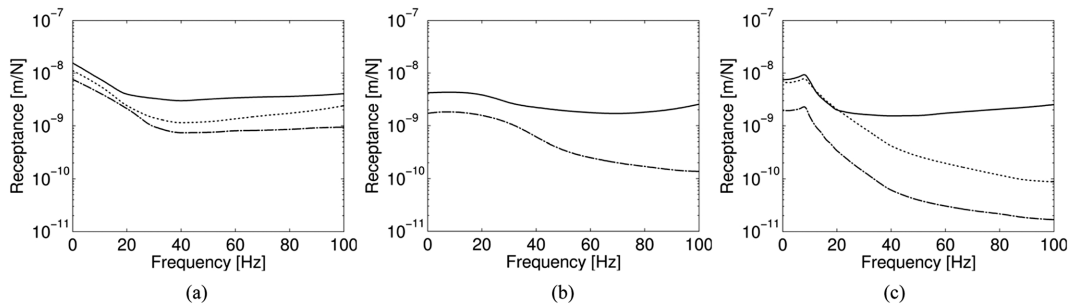

Fig. 9 Receptance of the rail (solid line), the sleeper (dotted line) and the track-soil interface (dashed-dotted line) for (a) the ballast track, (b) the slab track and (c) the floating slab track

load transmission from the tracks to the soil (Galvín *et al*. 2010b). The ballasted track presents two flexibility levels, the rail pads and the ballast layer, while the conventional slab track only has the flexibility level provided by the rail pads. Due to that, in the case of the ballasted track, the rail, the sleeper and the track-soil interface have similar displacements, whereas in the slab track the displacements at the rail level are much higher than the others. For a slab track, the track-soil interface displacements match up with the sleeper displacements. In a floating slab track, the insertion of the slab mat causes an increase of the displacement around the isolation frequency. In comparison with the unisolated slab track, the floating slab track presents higher rail displacements around the isolation frequency. After that, the rail has a similar response in both tracks. In a similar way, an amplification of the response of the sleeper and the track-soil interface occurs around the isolation frequency of the slab track. However, the isolated slab track presents track-soil interface displacements much lower than the unisolated track at frequencies higher than about 20 Hz. It can be concluded that an effective control of the track-soil interface vibrations is achieved at frequencies sufficiently higher than the isolation frequency, while vibrations increase at lower frequencies.

Figs. 10-12 compare the track and the free field displacements for the ballast track, the unisolated slab track and the isolated slab track due to a single axle travelling at $v = 250$ km/h, $v = 280$ km/h and $v = 315$ km/h, respectively. The results are shown on the same scale. Fig. 10 shows the track and soil behaviour for a train speed lower than the Rayleigh wave velocity in the soil. In this case, the vertical soil displacements are almost symmetric with respect to the moving load. Track induced vibrations in ballasted and floating slab tracks are higher than in the slab track. The radiation of waves from the track to the soil varies with the type of track. The effect of the load is concentrated in the ballast track, but it spreads through both the slab track and the floating slab track. If the soil and track behaviour of the ballasted track is compared for the three speeds (Figs. 10(a), 11(a) and 12(a)), it can be observed that the symmetry of the soil motion is lost as axle speed increases due to the radiation effect of the Mach waves, and the soil displacements are amplified for $v = 280$ km/h (Fig. 11(a)), which is close to the critical speed of this system. This effect is not observed in the slab tracks that remain in the same condition due to the lower flexibility of the systems (Figs. 10(b,c), 11(b,c) and 12(b,c)).

4.3 Vibrations induced by high-speed train passage in a transition zone between ballast and slab track

The proposed numerical model is used in this section to study the dynamic behaviour of a transition zone between a ballast track and a slab track (Galvín *et al*. 2010a), which is frequently located at tunnel entrances or near railway stations.

The ballasted track system considered (Fig. 8(a)) is composed of two layers: a ballast layer over a sub-ballast layer. The ballast has a density $\rho = 1500$ kg/m^3, a Poisson ratio $v = 0.2$ and a Young's modulus $E = 280 \times 10^6$ N/m^2.

The sub-ballast layer has a density $\rho = 1500$ kg/m^3, a Poisson ratio $v = 0.2$ and a Young's modulus $E = 140 \times 10^6$ N/m^2. The rail pads have a thickness of 10 mm and the stiffness and damping values are $k_{rp} = 150 \times 10^6$ N/m and $c_{rp} = 13.5 \times 10^3$ Ns/m.

The considered slab track system (Fig. 8(b)) is composed of two UIC60 rails supported by pre-stressed concrete mono-block sleepers separated $d = 0.60$ m. The concrete slab has a density $\rho = 2500$ kg/m^3, a Poisson ratio $v = 0.2$ and a Young's modulus $E = 34 \times 10^9$ N/m^2. A hydraulic subbase is placed below the concrete slab in order to reduce gradually the transmitted forces from

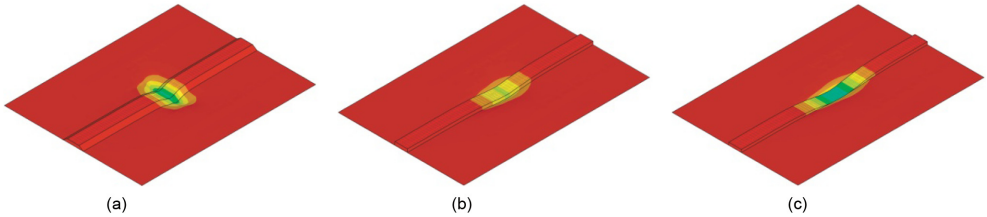

Fig. 10 Track and free field displacements due to a single axle travelling at $v = 250$ km/h for (a) the ballast track, (b) the unisolated slab track and (c) the isolated slab track

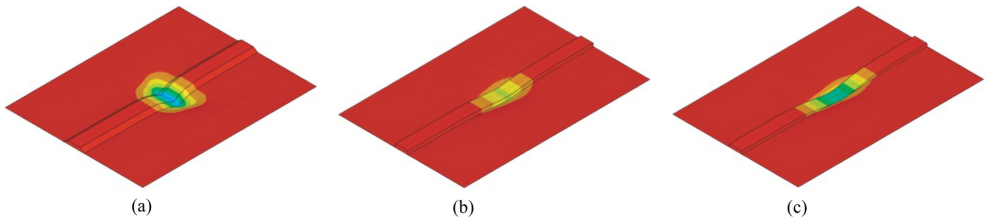

Fig. 11 Track and free field displacements due to a single axle travelling at $v = 280$ km/h for (a) the ballast track, (b) the unisolated slab track and (c) the isolated slab

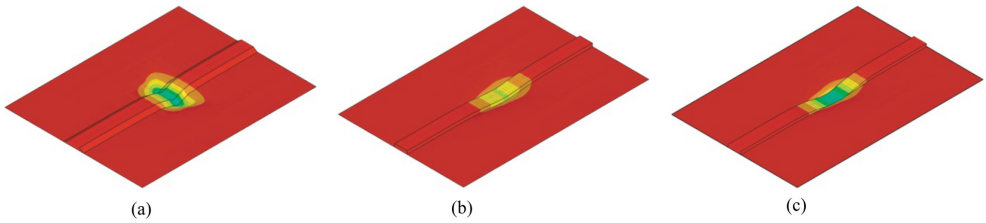

Fig. 12 Track and free field displacements due to a single axle travelling at $v = 315$ km/h for (a) the ballast track, (b) the unisolated slab track and (c) the isolated slab track

the track to the subgrade. The hydraulic subbase has a density $\rho = 2500$ kg/m^3, a Poisson ratio $v = 0.2$ and a Young's modulus $E = 10 \times 10^9$ N/m^2, and the same width as the concrete slab.

Slab tracks have a higher stiffness as compared to ballasted tracks and, because of that a transition zone between ballasted and slab track must be carefully designed to make a gradual change of the stiffness to ensure track quality and passenger comfort. Fig. 13(a) shows the geometry of the transition zone between ballasted and slab track. In the transition slab track zone the thickness of the hydraulic subbase layer increases from 0.3 m to 0.46 m. After that, the hydraulic sub-base layer replaces the sub-ballast layer under the ballast layer in the transition ballasted track zone. By doing so, the stiffness changes between the different parts of the transition zone are smoother. The discretization of the transition zone employed is shown in Fig. 13(b). The track and soil response are studied at four sections. Section A is located in the ballasted track 3 m before the transition zone. Section B corresponds to the middle of the ballasted transition zone and section C to the middle of slab track transition. Finally, section D is located in the slab track 9 m from the transition zone.

An analysis of the transition zone between ballast and slab track is made comparing the computed vibrations obtained with the discretization shown in Fig. 13(b), and the obtained results using four independent track-soil models that represent each section. Fig. 14 compares the results from the

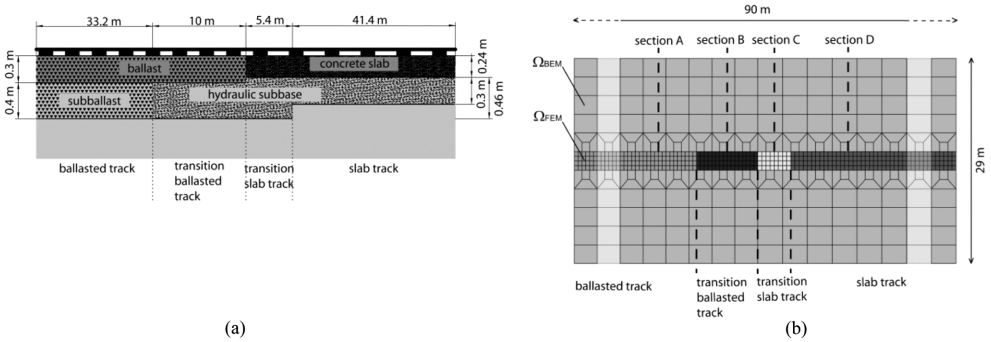

Fig. 13 Transition zone model: (a) geometry and (b) discretization

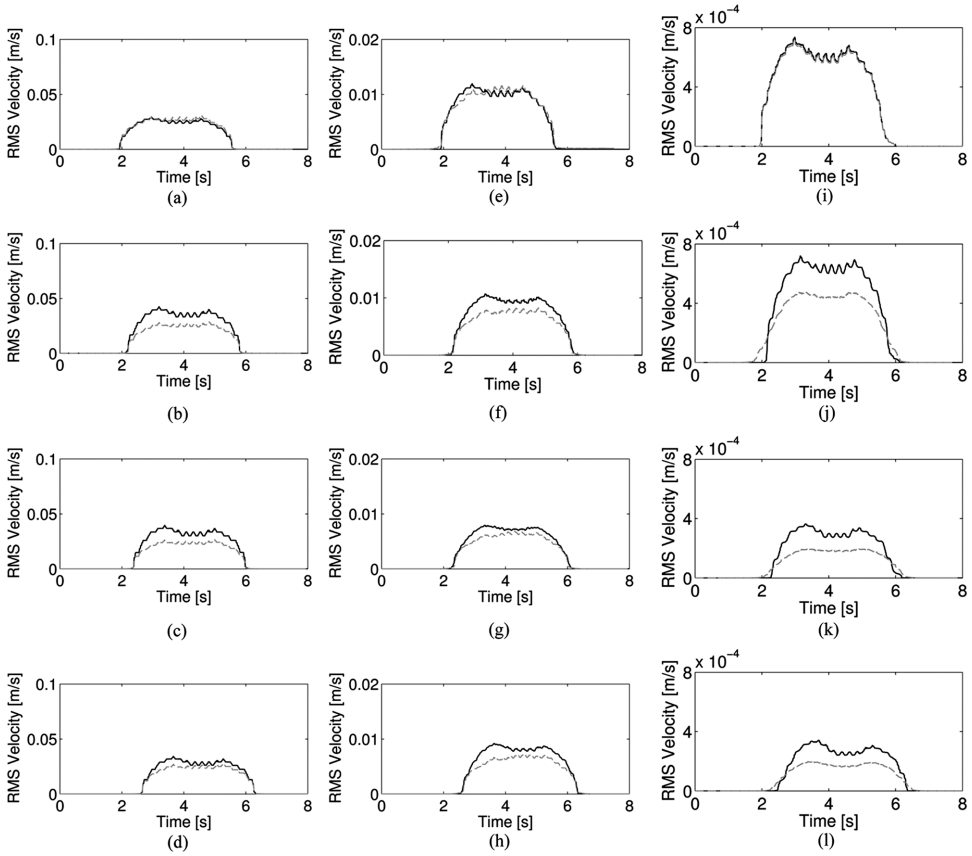

Fig. 14 Running RMS value of the vertical velocity (a-d) at the rail, (e-h) the sleeper and (i-l) at a point in the free field located at 11.8 m from track axis for the medium soil and the medium rail pad computed from the transition zone model (Fig. 13) (black line) and from an invariant geometry model (dashed grey line) at a train speed $v = 298$ km/h travelling on: (a,e,i) section A, (b,f,j) section B, (c,g,k) section C and (d,h,l) section D

transition zone model (using the present three-dimensional model) and an invariant geometry model (using the present three-dimensional model with track and soil invariant in the track direction). The

results obtained for both models in section A are similar. As the train goes into the transition zone the vertical stiffness of the track is modified. Rail, sleeper and free-field response is increased due to the inertial forces induced by the effect of the vehicle passage and the stiffness track changes. The transient response disappears as the train travels along the slab track. The correlation between the computed results from both models in the transition zone present is not good and three-dimensional models should be used to obtain an accurate response for these problems.

5. Short-span railway bridges

This section analyses the effect of soil-structure interaction on railway bridges. The dynamic behaviour and the resonant response of the coupled bridge-soil system are studied (Romero *et al*. 2012).

A simple supported railway bridge of 12 m length is studied. The deck is composed of 0.25 m thickness concrete slab. The slab resting over five pre-stressed concrete beams with 0.75×0.3 m rectangular crosssection. A distance 1.39 m between beams is considered. The concrete has density $\rho = 2500$ kg/m^3, Poisson's ratio $v = 0.2$ and Young's modulus $E = 31 \times 10^9$ N/m^2.

The deck leans over two concrete abutments with density $\rho = 2500$ kg/m^3, Poisson's ratio $v = 0.3$ and Young's modulus $E = 20 \times 10^9$ N/m^2. Beams are resting on laminated rubber bearings. The bearings have thickness equal to 20 mm and the stiffness and damping values are $k_b = 560 \times 10^6$ N/m and $c_b = 50.4 \times 10^3$ Ns/m, respectively.

A single ballast track is located over the deck. The track is composed of two UIC60 rails with a bending stiffness $EI = 6.45 \times 10^6$ N/m^2 and a mass per unit length $m = 60.3$ kg/m for each rail. The rail pads have a 10 mm thickness and their stiffness and damping values are $k_{rp} = 150 \times 10^6$ N/m and $c_{rp} = 13.5 \times 10^3$ Ns/m, respectively. The pre-stressed concrete mono-block sleepers have length $l = 2.60$ m, width $w = 0.235$ m, height $h = 0.205$ m and mass $m = 300$ kg. A distance $d = 0.6$ m between the sleepers is considered. The ballast has density $\rho = 1800$ kg/m^3, Poisson ratio $v = 0.2$ and Young's modulus equal to $E = 209 \times 10^6$ N/m^2. The width of the ballast equals 2.92 m and the height $h = 0.7$ m.

The structure is assumed to be located at the surface of a homogeneous half-space that represents the soil. The soil is an homogeneous viscoelastic soil with Poisson's ratio $v = 0.35$, mass density $\rho = 1800$ kg/m^3 and two different *S*-wave velocities: $C_s = \infty$ and $C_s = 400$ m/s, corresponding to an infinity stiffness soil and a stiff soil, respectively.

Table 1 shows the natural frequencies and mode shapes of the structure. The first resonant frequency of the structure moves to $f_1 = 11.01$ Hz when soil-bridge interaction is taken into account. The damping ratio, obtained from the free vibration response, reaches a value $\zeta = 6.4\%$ when soil-structure interaction (SSI) is accounted for. A value $\zeta = 2\%$ is obtained when interaction is not considered.

Table 1 Mode shapes and resonant frequencies (SSI is not considered)

Mode shape	Frequency Hz	Type
1	11.80	First bending (symmetric)
2	21.90	First torsional
3	29.99	First bending of the cross-section (symmetric)
4	47.82	First antisymmetric bending

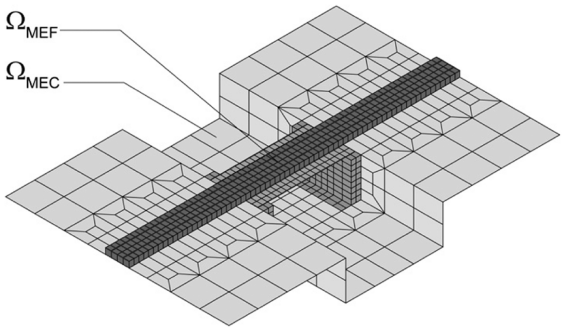

Fig. 15 Soil-structure discretization

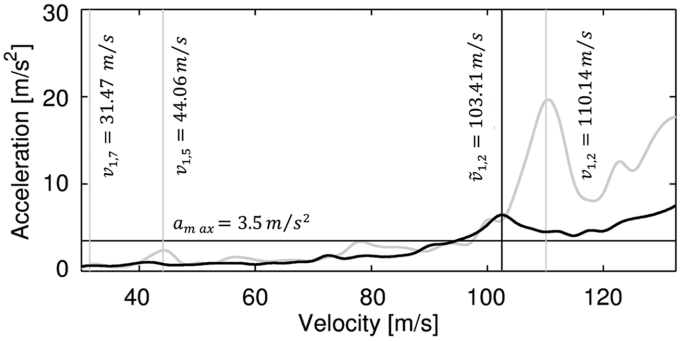

Fig. 16 Maximum vertical acceleration at the mid-span center deck for $C_s = \infty$ m/s (grey line) and $C_s = 400$ m/s (black line)

The resonant condition of a bridge excited by a row of moving forces can be expressed as follows (Frýba 2001, Xia *et al*. 2006).

$$v_{n,i} = \frac{f_n d}{i} \qquad (n = 1,2,\ldots, i = 1,2,\ldots) \tag{6}$$

where, $v_{n,i}$ is the train speed, f_n is the $n-th$ resonant frequency of the bridge and d is a characteristic distance between moving loads. Fig. 16 shows the maximum vertical acceleration at the centre of mid-span deck for a Alstom HST passages at speeds between 30 m/s and 130 m/s (108 km/h and 468 km/h, respectively). It is observed as the deck acceleration increases with the train speed. A local maximum is reached at the resonant speed for the first bending mode shape, considering the distance $d = 18.7$ m between boogies. Fig. 16 shows maximum vibration levels at the speed $v_{1,2} = 110.4$ m/s when soil-bridge interaction is not considered. The maximum acceleration at the center of the mid-span deck is below $a_{max} = 3.5$ m/s^2 in the range of operating speeds on current high speed lines, which is the limit given by the European Committee for Standardisation (CEN) (2002). The response of the structure changes substantially when soil-structure interaction is considered. The second resonant speed of the first mode shape decreases to $\tilde{v}_{1,2} = 103$ m/s when soil-bridge interaction is accounted for. Moreover, it is observed that the maximum level of acceleration achieved in the resonant regime is significantly lower when soil-structure interaction is considered.

6. Conclusions

In this paper, a review of recent advances in a numerical model to predict vibrations due to train passage has been presented. The numerical model is based on time domain three-dimensional finite element and boundary element formulations. The formulation allows taking into account local soil discontinuities, underground constructions and nearby structures that break the uniformity of the geometry along the track line. Track and other structures are modelled using the finite element method and their non-linear behaviour could be considered because a time domain formulation is employed. The soil is represented using the boundary element method, where a full space fundamental solution is used in combination with quadratic boundary elements. The train vehicle is modelled as a multi-body and, therefore, the quasi-static and the dynamic excitation mechanisms can be considered, taking into account the dynamic effects due to discrete sleeper support and the wheel and rail irregularities.

The influence of the quasi-static and the dynamic loading contribution has been presented, concluding:

1. Vehicle mass model should be considered to predict accurately the quasi-static response.
2. The suspended mass should be taken into account in order to predict the track and soil response due the dynamic contribution at low frequencies.

Track-soil interaction has been presented for ballasted and non-ballasted tracks. It can be concluded from the computed results:

1. Ballast and embankment have a significant influence on the system response.
2. The critical speed for a ballast track is close to the Rayleigh wave velocity in the soil.
3. For non-ballasted track, it is not observed that the critical system speed is reached.
4. The insertion of a resilient material in a slab track leads to an amplification of the response at frequencies around the isolation frequency. Above this frequency, a reduction of the response is attained.
5. A transition zone between ballast and slab track must be carefully analysed to predict the dynamic effect due to the stiffness changes along the track.

Finally, the resonance condition on railway bridges depends on the resonance frequencies. The resonant velocities are lower when soil-bridge interaction is considered and the amplification on resonant regime is lower.

All results demonstrate the capabilities and robustness of the numerical approach which is very well suited for the dynamic analysis of complex soil-train-structure interaction problems.

Acknowledgments

This research is financed by the Ministerio de Ciencia e Innovación of Spain under the research Project BIA2010-14843. The financial support is gratefully acknowledged.

References

Metrikine, A. and Popp, K. (1999), "Instability of vibrations of an oscillator moving along a beam on an elastic half-space", *Eur. J. Mech. A-Solid.*, **18**(2), 331-349.

Metrikine, A. and Popp, K. (1999), "Vibration of a periodically supported beam on an elastic half-space", *Eur. J. Mech. A-Solid*., **18**(4), 679-701.
Metrikine, A., Verichev, S. and Blauwendraad, J. (2005), "Stability of a two-mass oscillator moving on a beam supported by a viscoelastic half-space", *Int. J. Solids Struct*., **42**(3-4), 1187-1207.
Pesterev, A., Bergman, L., Tan, C., Tsao, T.C. and Yang, B. (2003), "On asymptotics of the solution of the moving oscillator problem", *J. Sound Vib*., **260**(3), 519-536.
Romero, A., Domínguez, J. and Galvín, P. (2012), *Comportamiento dinámico de viaductos cortos considerando la interacción vehículo-vía-estructura-suelo*, Revista Internacional de Métodos Numéricos para Cálculo y Diseño en Ingeniería, **28**(1), 55-63.
Olmos, B.A. and Roësset, J.M. (2010), "Effects of the nonlinear behavior of lead-rubber bearings on the seismic response of bridges", *Earthq. Struct*., **1**(2), 215-230.
Esveld, C. (2001), *Modern railway track*, MRT Productions, Zaltbommel.
Banister, D. and Hall, P. (1993), "The second railway age", *Built Environ*., **19**(3-4), 157-162.
Karabalis, D. and Beskos, D. (1985), "Dynamic response of 3-D flexible foundations by time domain BEM and FEM", *Soil Dyn. Earthq. Eng*., **4**(2), 91-101.
European Committee for Standardisation (CEN) (2002), *Eurocode 1: Actions on structures. Part 2: traffic loads on bridges*, Final Draft prEN 1991-2 (pre-European Standard).
Lombaert, G. and Degrande, G. (2009), "Ground-borne vibration due to static and dynamic axle loads of intercity and highspeed trains", *J. Sound Vib*., **319**(3-5), 1036-1066.
Lombaert, G., Degrande, G., Kogut, J. and Francois, S. (2006), "The experimental validation of a numerical model for the prediction of railway induced vibrations", *J. Sound Vib*., **297**(3-5), 512-535.
Dieterman, H. and Metrikine, A. (1996), "The equivalent stiffness of a halfspace interacting with a beam. Critical velocities of a moving load along the beam", *Eur. J. Mech. A-Solid*., **15**(1), 67-90.
Xia, H. Zhang, N. and Guo, W. (2006), "Analysis of resonance mechanism and conditions of train-bridge system", *J. Sound Vib*., **297**(3-5), 810-822.
Xia, H., Cao, Y. and De Roeck, G. (2010), "Theoretical modeling and characteristic analysis of moving-train induced ground vibrations", *J. Sound Vib*., **329**(7), 819-832.
Takemiya, H. and Bian, X. (2005), "Substructure simulation of inhomogeneous track and layered ground dynamic interaction under train passage", *J. Eng. Mech*., **131**(7), 699-711.
International Organization for Standardization, ISO 8608 (1995), *1995 Mechanical vibration road surface profilesreporting of measured data.*
Domínguez, J. (1993), *Boundary elements in dynamics*, Computational Mechanics Publications and Elsevier Applied Science, Southampton.
Knothe, K. and Grassie, S. (1993), "Modelling of railway track and vehicle/track interaction at high frequencies", *Vehicle Syst. Dyn*., **22**(3-4), 209-262.
Auersch, L. (2005), "The excitation of ground vibration by rail traffic: Theory of vehicle-track-soil interaction and measurements on high-speed lines", *J. Sound Vib*., **284**(1-2), 103-132.
Auersch, L. (2008), "The effect of critically moving loads on the vibrations of soft soils and isolated railway tracks", *J. Sound Vib*., **310**(3), 587-607.
Frýba, L. (2001), "A rough assessment of railway bridges for high-speed trains", *Eng. Struct*., **23**(5), 548-556.
Adam, M., Pflanz, G. and Schmid, G. (2000), "Two- and three-dimensional modelling of half-space and train-track embankment under dynamic loading", *Soil Dyn. Earthq. Eng*., **19**(8), 559-573.
Hauck, M., Wettschureck, G. and Heckl, R. (1996), "Structure-borne sound and vibration from rail traffic", *J. Sound Vib*., **193**(1), 175-184.
Marrero, M. and Domínguez, J. (2003), "Numerical behavior of time domain BEM for three-dimensional transient elastodynamic problems", *Eng. Anal. Bound. Elem*., **27**(1), 39-48.
Newmark, N. (1959), "A method of computation for structural dynamics", *J. Eng. Mech.-ASCE*, **85**(1) 67-94.
von Estorff, O. and Pabrucki, M. (1990), "Dynamic response in the time domain by coupled boundary and finite elements", *Comput. Mech*., **6**(1), 35-46.
Zienkiewicz, O. (1986), *The finite element method*, 3rd Edition, McGraw-Hill.
Galvín, P. and Domínguez, J. (2007a), "High-speed train-induced ground motion and interaction with structures", *J. Sound Vib*., **307**(3-5), 755-777.

Galvín, P. and Domínguez, J. (2007b), "Analysis of ground motion due to moving surface loads induced by high-speed trains", *Eng. Anal. Bound. Elem*., **31**(11), 931-941.
Galvín, P. and Domínguez, J. (2009), "Experimental and numerical analyses of vibrations induced by high-speed trains on the Córdoba-Málaga line", *Soil Dyn. Earthq. Eng*., **29**(4), 641-657.
Galvín, P., Romero, A. and Domínguez, J. (2010a), "Fully three-dimensional analysis of high-speed train-track-soil-structure dynamic interaction", *J. Sound Vib*., **329**(24), 5147-5163.
Galvín, P., Romero, A. and Domínguez, J. (2010b), "Vibrations induced by HST passage on ballast and non-ballast tracks", *Soil Dyn. Earthq. Eng*., **30**(9), 862-873.
Galvín, P., François, S., Schevenels, M., Bongini, E., Degrande G. and Lombaert, G. (2010), "A 2.5D coupled FE-BE model for the prediction of railway induced vibrations", *Soil Dyn. Earthq. Eng*., **30**(12), 1500-1512.
Krylov, V. (1994), "On the theory of railway-induced ground vibrations", *J. Phys*., **4**(5), 769-772.
Krylov, V. (1995), "Generation of ground vibrations by superfast trains", *Appl. Acoust*., **44**(2), 149-164.
Sheng, X., Jones, C. and Thompson, D. (2003), "A comparison of a theoretical model for quasi-statically and dynamically induced environmental vibration from trains with measurements", *J. Sound Vib*., **267**(3), 621-635.
Sheng, X., Jones, C. and Thompson, D. (2004), "A theoretical model for ground vibration from trains generated by vertical track irregularities", *J. Sound Vib*., **272**(3-5), 937-965.
Sheng, X., Jones, C. and Thompson, D. (2006), "Prediction of ground vibration from trains using the wavenumber finite and boundary element methods", *J. Sound Vib*., **293**(3-5), 575-586.

SA